

Heteroscedastic sparse high-dimensional linear regression with a partitioned empirical Bayes ECM algorithm

Anja Zgodic^a, Ray Bai^b, Jiajia Zhang^a, Yuan Wang^a,
Chris Rorden^c, Alexander C. McLain^{a*}

^aDepartment of Epidemiology and Biostatistics,

^bDepartment of Statistics,

^cDepartment of Psychology

University of South Carolina

September 19, 2023

Abstract

Sparse linear regression methods for high-dimensional data often assume that residuals have constant variance. When this assumption is violated, it can lead to bias in estimated coefficients, prediction intervals with improper length, and increased type I errors. This paper proposes a heteroscedastic (H) high-dimensional linear regression model through a partitioned empirical Bayes Expectation Conditional Maximization (H-PROBE) algorithm. H-PROBE is a computationally efficient maximum *a posteriori* (MAP) estimation approach based on a Parameter-Expanded Expectation-Conditional-Maximization (PX-ECM) algorithm. It requires minimal prior assumptions on the regression parameters through plug-in empirical Bayes estimates of hyperparameters. The variance model uses recent advances in multivariate log-Gamma distribution theory and can include covariates hypothesized to impact heterogeneity. The motivation of our approach is a study relating Aphasia Quotient (AQ) to high-resolution T2 neuroimages of brain damage in stroke patients. AQ is a vital measure of language impairment and informs treatment decisions, but it is challenging to measure and subject to heteroscedastic errors. As a result, it is of clinical importance – and the goal of this paper – to use high-dimensional neuroimages to predict and provide prediction intervals for AQ that accurately reflect the heterogeneity in the residual variance. Our analysis demonstrates that H-PROBE can use markers of heterogeneity to provide prediction interval widths that are narrower than standard methods without sacrificing coverage. Further, through extensive simulation studies, we exhibit that the proposed approach results in superior prediction, variable selection, and predictive inference than competing methods.

Keywords: Bayesian variable selection, ECM algorithm, empirical Bayes, heteroscedasticity, high-dimensional linear regression.

*Corresponding author: alex.mclain@sc.edu

1 Introduction

Much of the current literature on sparse linear regression methods for high-dimensional data assumes that the residuals have a constant variance. However, in practice, this assumption is often violated. A clinical application where high-dimensional heteroscedastic data arises is in treatment decisions for neurological disorders based on patient imaging data. Johnson et al. (2019) present results from a study on language rehabilitation in patients who experienced a left-hemispheric stroke and suffer from aphasia – a language disorder impacting speech. The outcome of interest is the subjects’ Aphasia Quotient (AQ), a score quantifying language impairment that is vital to understanding patients’ treatment options (Risser and Spreen, 1985). However, collecting AQ is a cumbersome task, particularly for patients who have recently had a stroke (Odekar and Hallowell, 2005). Consequently, it is of interest to develop a model that can predict and provide prediction intervals for AQ based on subjects’ brain imaging (Yourganov et al., 2015). Brain images are obtained through T1 structural Magnetic Resonance Imaging (MRI) and give the lesion status (i.e., damaged or not damaged from stroke) of more than 5×10^6 three-dimensional (1 mm^3) brain voxels. Patients with little brain damage commonly score near the top of the range (0 – 100). More substantial damage results in lower AQ scores on average, but some subjects exhibit notable resilience with relatively high AQ (as displayed in Figure 5). As a result, the total number of damaged voxels is hypothesized to have a positive relationship with the residual variance.

If ignored, heterogeneity can harm multiple areas of analyses, including bias in estimated coefficients, prediction intervals with improper length, and increased type I errors (Carroll and Ruppert, 1988). These drawbacks can be particularly impactful in high-dimensional settings where the number of predictors is much larger than the sample size,

and heterogeneity can lead to overfitting. Penalized linear regression techniques have been expanded for data displaying non-constant errors. These methods are designed to down-weight outliers or anomalous observations with large error variances. Proposals include methods that weight the objective function of the Least Absolute Shrinkage and Selection Operator (LASSO) (Ziel, 2016) using Least Absolute Deviation (LAD) (Wang et al., 2007) or the square-root of the residual sum of squares (Belloni et al., 2014). In a similar fashion, a sparse version of least trimmed squares (LTS) was proposed where the sum of the order statistics of squared residuals is minimized with a LASSO-type penalty (Rousseeuw, 1984; Rousseeuw and Van Driessen, 2006; Alfons et al., 2013).

The aforementioned methods may not be suited for scenarios where there are known factors hypothesized to be related to heterogeneity in the data. To address this gap, a second line of research specifically focuses on modeling the variance of observations. We have located only three such proposals for the high-dimensional setting, all in the frequentist framework. First, Daye et al. (2012) proposed doubly regularized likelihood estimation with ℓ_1 penalty on parameters for both the mean and variance. Similarly, Chiou et al. (2020) uses a multi-step orthogonal greedy algorithm (Temlyakov, 2000) and backward elimination to select variables for the models on the mean and the variance. Finally, Zhou and Zou (2021) leverage Daye et al.’s conceptual framework but use sample splitting to select predictors via LASSO models on the mean, obtain cross-sample residuals, and fit additional LASSO models to the residual variance.

While many of the above methods can sufficiently incorporate heteroscedasticity in the high-dimensional setting, none of the methods have utilized the Bayesian variable selection framework or investigated creating prediction intervals for future observations. The latter issue is important in heteroscedastic models since the lengths of prediction intervals may

vary by known factors that are available in the data. Conformal inference methods (Vovk et al., 2005; Lei et al., 2018; Tibshirani and Foygel, 2019), which can be used with penalized regression, come with guaranteed finite-sample coverages of prediction intervals. However, such guarantees are marginal and may be higher or lower with some predictor combinations. Marginal properties are unsatisfactory for heterogeneous data, particularly when sources of heterogeneity are known.

In light of these limitations, we propose a heteroscedastic (H) high-dimensional linear regression through a partitioned empirical Bayes Expectation Conditional Maximization (H-PROBE) algorithm. Our approach provides predictions for new observations and addresses a crucial gap in previous heteroscedastic methods, i.e., a lack of procedures to estimate prediction intervals. We remedy this drawback by basing H-PROBE upon the previously established PROBE framework (McLain et al., 2022). PROBE is a computationally efficient maximum *a posteriori* (MAP) estimation approach based on a quasi Parameter-Expanded Expectation Conditional Maximization (PX-ECM) algorithm (Meng and Rubin, 1993; Liu et al., 1998). It requires minimal prior assumptions on the regression parameters through the use of plug-in empirical Bayes estimates of hyperparameters in the E-step, which is motivated by the popular two-group approach to multiple testing (Efron et al., 2001). H-PROBE expands PROBE by utilizing recent advances in heterogeneous Bayesian modeling via multivariate log-Gamma distribution theory (Bradley et al., 2020; Parker et al., 2021).

To the best of our knowledge, H-PROBE is the first Bayesian approach in high-dimensional modeling, including both models on the mean and the variance. The novel contributions of H-PROBE are (i) modeling of the mean and variance within the same Bayesian framework with variable selection in the mean parameters, (ii) predictive capabilities for heteroscedas-

tic data, including prediction intervals, and (iii) incorporating non-sparse predictors into the mean. The remaining paper layout is as follows. We describe H-PROBE in Section 2 and numerical studies evaluating its performance in Section 3. Section 4 presents a comprehensive analysis of the AQ imaging study, and Section 5 concludes with a brief discussion.

2 Methods

2.1 Model framework

In most linear regression models with outcome $\mathbf{Y} = (Y_1, Y_2, \dots, Y_n)$, predictors $\mathbf{X} = (\mathbf{X}_1, \dots, \mathbf{X}_p)$, and error term $\boldsymbol{\epsilon} = (\epsilon_1, \epsilon_2, \dots, \epsilon_n)$, it is assumed that $Var(\epsilon_i) = \sigma^2$ for all $i = 1, \dots, n$. As a result, the error term has the same variance for all observations (homoscedasticity). In a contrasting scenario, the error term may display a variance that differs from observation to observation. Then, the linear regression model for heteroscedastic data is written as

$$Y_i = \mathbf{X}_i \mathbf{b} + \epsilon_i, \tag{1}$$

where $\mathbf{b} \in \mathbb{R}^p$, $E(\epsilon_i) = 0$, and $Var(\epsilon_i) = \sigma_i^2$. Let X_{ik} represent predictor k for observation i , with $n \times 1$ vector $\mathbf{X}_k = (X_{1k}, \dots, X_{nk})$, $n \times p$ design matrix \mathbf{X} , and $Var(\boldsymbol{\epsilon}) = \boldsymbol{\Sigma} = \text{diag}(\sigma_1^2, \dots, \sigma_n^2)$ as a diagonal $n \times n$ matrix. Assuming Gaussian errors the distribution of the outcome is $\mathbf{Y} \sim N(\mathbf{X}\mathbf{b}, \boldsymbol{\Sigma})$.

We leverage a Bayesian framework to accommodate a high-dimensional ($p \gg n$) setting and conduct sparse linear regression. Specifically, our model will allow for sparse and non-sparse predictors. For ease of presentation, we assume the mean's non-sparse predictors are also the variance predictors, denoted by $\mathbf{V} \in \mathbb{R}^{n \times v}$. In practice, this need not be the

case. With this we rewrite the model in (1) as

$$\mathbf{Y} = \mathbf{X}(\boldsymbol{\gamma}\boldsymbol{\beta}) + \mathbf{V}\boldsymbol{\varphi} + \boldsymbol{\epsilon}, \quad (2)$$

where $\boldsymbol{\gamma}\boldsymbol{\beta}$ is a Hadamard product, $\boldsymbol{\gamma} \in \{0, 1\}^p$, and $\boldsymbol{\varphi} \in \mathbb{R}^v$. Let $\mathcal{D} = \{\mathcal{D}_1, \dots, \mathcal{D}_n\}$ with $\mathcal{D}_i = (Y_i, \mathbf{X}_i, \mathbf{V}_i)$ denote the observed data. We add the following parametric model on the diagonal variance matrix $\boldsymbol{\Sigma}$,

$$-\log\{\text{diag}(\boldsymbol{\Sigma})\} = \mathbf{V}\boldsymbol{\omega}, \quad (3)$$

where $\boldsymbol{\omega} \in \mathbb{R}^v$. The log transformation on the variances ensures positivity, can accommodate variances that vary over orders of magnitude, and has been long established in variance function modeling (Carroll, 1988; Cleveland, 1993). The complete Bayesian framework includes prior information on

$$\begin{aligned} p(\boldsymbol{\beta}) &= \prod_{k=1}^p f_{\beta}(\beta_k), \\ p(\boldsymbol{\gamma}|\boldsymbol{\pi}) &= \pi^{p-|\boldsymbol{\gamma}|}(1-\pi)^{|\boldsymbol{\gamma}|}, \\ p(\boldsymbol{\varphi}) &\propto 1, \\ \boldsymbol{\omega} &\sim \text{MLG}(\mathbf{0}, c^{1/2}\sigma_{\omega}^2\mathbf{I}, c\mathbf{1}, c\mathbf{1}), \end{aligned}$$

where MLG denotes the Multivariate Log Gamma distribution with $c, \sigma_{\omega}^2 > 0$. The MLG distribution yields conjugate conditional posteriors in heteroscedastic linear models (Parker et al., 2021). MLG distributions are useful in contexts where both Gaussian priors and computational efficiency are desired. The MLG prior converges to a multivariate normal prior with mean $\mathbf{0}$ and variance $\sigma_{\omega}^2\mathbf{I}$ as the value of c approaches infinity (Bradley et al.,

2020; Parker et al., 2021). Throughout, we use $\sigma_\omega^{-1} = 0$ and $c = 1000$ to yield a weakly informative prior on ω .

To obtain the posterior distributions for parameters, we assume $f_\beta \propto 1$ and $\pi \sim \text{Uniform}(0, 1)$. In practice, we leave hyperparameters π and f_β unspecified and estimate them using plug-in empirical Bayes estimators (Section 2.4). To obtain the conditional posterior distribution of β , we split (\mathbf{X}, β) into $(\mathbf{X}_\gamma, \beta_\gamma)$ when $\gamma_k = 1$ and $(\mathbf{X}_{\bar{\gamma}}, \beta_{\bar{\gamma}})$ when $\gamma_k = 0$. Conditional on γ and ω (i.e., Σ), the posterior distribution of $\gamma\beta$ and φ is

$$\begin{pmatrix} \beta_\gamma \\ \varphi \end{pmatrix} \Big| (\mathcal{D}, \omega, \gamma) \sim N \left\{ (\mathbf{U}'_\gamma \Sigma^{-1} \mathbf{U}_\gamma)^{-1} \mathbf{U}'_\gamma \Sigma^{-1} \mathbf{Y}, (\mathbf{U}'_\gamma \Sigma^{-1} \mathbf{U}_\gamma)^{-1} \right\}$$

where $\mathbf{U}_\gamma = (\mathbf{X}_\gamma \mathbf{V})$, while $\beta_{\bar{\gamma}} | (\mathcal{D}, \omega, \gamma) \sim \delta_0(\cdot)$ a point mass at zero. Given β , γ , and φ the posterior for ω has density

$$f_\omega(\omega) \propto \exp \{ \mathbf{c}'_\omega \mathbf{H}_\omega \omega - \kappa'_\omega \exp(\mathbf{H}_\omega \omega) \}, \quad (4)$$

which is proportional to a $MLG(\mathbf{0}, \mathbf{H}_\omega, \mathbf{c}_\omega, \kappa_\omega)$ distribution with

$$\mathbf{H}_\omega = \begin{bmatrix} \mathbf{V} \\ c^{-1/2} \sigma_\omega^{-1} \mathbf{I}_v \end{bmatrix}, \quad \mathbf{c}_\omega = \left(\frac{1}{2} \mathbf{1}'_n, c \mathbf{1}'_v \right)', \quad \text{and} \quad \kappa_\omega = \left(\frac{1}{2} \|\mathbf{Y} - \mathbf{X}(\gamma\beta) - \mathbf{V}\varphi\|^2, c \mathbf{1}'_v \right)',$$

where \mathbf{I}_v denotes a $v \times v$ identity matrix and $\mathbf{1}_v$ a $v \times 1$ vector of ones.

Within the EM algorithm, the parameter estimates at iteration t are used to obtain the expected complete-data log-posterior distribution with respect to γ ,

$$E_\gamma \left\{ \log p(\beta, \varphi, \omega | \mathcal{D}, \gamma) | \mathcal{D}, \beta^{(t)}, \varphi^{(t)}, \omega^{(t)} \right\},$$

which is sequentially maximized to obtain MAP estimates $\boldsymbol{\beta}^{(t+1)}$, $\boldsymbol{\varphi}^{(t+1)}$, and $\boldsymbol{\omega}^{(t+1)}$ (i.e., $\boldsymbol{\Sigma}^{(t+1)}$) (discussed in Sections 2.3 and 2.4). Finally, for γ_k , plug-in empirical Bayes estimators of π and f_β are used to estimate the posterior expectation $\mathbf{p} = (p_1, \dots, p_p)$ where $p_k = P(\gamma_k = 1 | \mathcal{D}, \pi)$ (discussed in Section 2.4).

2.2 Overview and notation

We begin this Section with an overview of the PROBE algorithm (McLain et al., 2022). The aim is to perform MAP estimation for $\boldsymbol{\gamma}$, $\boldsymbol{\beta}$, $\boldsymbol{\varphi}$, and $\boldsymbol{\omega}$ in a high-dimensional setting. PROBE is based on a quasi Parameter-Expanded Expectation-Conditional-Maximization (PX-ECM) algorithm, which is a combination of the ECM and PX-EM algorithms (Meng and Rubin, 1993; Liu et al., 1998). The CM-step of the PX-ECM results in coordinate-wise (predictor-specific) optimization, where the remaining parameters are restricted to their values at the previous iteration. As a result, we partition the mean of the model (2) by predictor k . The notation $\mathbf{A}_{\setminus k}$ indicates the matrix, vector, or collection without predictor or element k . Define $\mathbf{W}_k = \mathbf{X}_{\setminus k}(\boldsymbol{\gamma}_{\setminus k}\boldsymbol{\beta}_{\setminus k}) + \mathbf{V}\boldsymbol{\varphi} = (W_{1k}, \dots, W_{nk})'$ and thus $E(\mathbf{Y} | \mathbf{W}_k) = \mathbf{X}_k\boldsymbol{\beta}_k + \mathbf{W}_k$, where \mathbf{W}_k encompasses the impact of all predictors except \mathbf{X}_k .

The above formulation is similar to Variational Bayes with the Coordinate-Ascent Variational Inference (CAVI) algorithm (Carbonetto and Stephens, 2012; Ray and Szabó, 2021). In these approaches, the expectation of \mathbf{W}_k is subtracted from the outcome when $\boldsymbol{\beta}_k$ is updated. Alternatively, since \mathbf{W}_k it is estimated as part of our algorithm, we use parameter-expansion (Liu et al., 1998) to include variables α_k which adjusts for the impact of \mathbf{W}_k when updating $\boldsymbol{\beta}_k$ for all $k = 1, \dots, p$. This results in

$$E(\mathbf{Y} | \mathbf{W}_k) = \mathbf{X}_k\boldsymbol{\beta}_k + \mathbf{W}_k\boldsymbol{\alpha}_k, \tag{5}$$

which simultaneously adjusts for the impact of \mathbf{X}_k and \mathbf{W}_k . The α_k parameter helps estimate the posterior variance of $\beta_k|\gamma_k = 1$ more accurately since it accounts for the dependence between \mathbf{W}_k and \mathbf{X}_k (discussed further in Section 2.3). This posterior variance is required in our implementation of the E-step and used to create prediction intervals in Section 2.6. For ease of presentation, we use a single \mathbf{W}_k and scalar α_k in our description of H-PROBE. The extension to multiple \mathbf{W}_k , each with its own expanded parameter is straightforward. For example, in our implementation of the method in simulations and data analyses, \mathbf{W}_k is split into sparse ($\mathbf{X}_{\setminus k}(\gamma_{\setminus k}\boldsymbol{\beta}_{\setminus k})$) and non-sparse ($\mathbf{V}\boldsymbol{\varphi}$) components with an expanded parameter on each component.

Each step of H-PROBE consists of estimating the MAP of $\boldsymbol{\varphi}$, $\boldsymbol{\omega}$, and then β_k given $\gamma_k = 1$ for all $k = 1, \dots, p$ in sequence. We assume an uninformative prior on α_k with $\alpha_k \sim f_\alpha \propto 1$. To obtain the MAP of β_k given $\gamma_k = 1$, let $\boldsymbol{\xi}_k = (\beta_k, \alpha_k)'$. Using $\mathbf{Z}_k = (\mathbf{X}_k \ \mathbf{W}_k)$ and conditioning on $\boldsymbol{\omega}$ (i.e., $\boldsymbol{\Sigma}$), the posterior is $\boldsymbol{\xi}_k|\mathcal{D}, \boldsymbol{\omega}, \gamma_k = 1 \sim N\{\hat{\boldsymbol{\xi}}_k, (q\mathbf{Z}'_k\boldsymbol{\Sigma}^{-1}\mathbf{Z}_k)^{-1}\}$, with $\hat{\boldsymbol{\xi}}_k = (\hat{\beta}_k, \hat{\alpha}_k)' = (\mathbf{Z}'_k\boldsymbol{\Sigma}^{-1}\mathbf{Z}_k)^{-1}\mathbf{Z}'_k\boldsymbol{\Sigma}^{-1}\mathbf{Y}$. Specifically, for the parameter of interest β_k , this gives the posterior $\beta_k|\mathcal{D}, \boldsymbol{\omega}, \gamma_k = 1 \sim N(\hat{\beta}_k, \hat{S}_k^2)$ where \hat{S}_k^2 is the (1,1) element of $(q\mathbf{Z}'_k\boldsymbol{\Sigma}^{-1}\mathbf{Z}_k)^{-1}$.

Note that \mathbf{W}_k is unknown since it is a function of $(\boldsymbol{\beta}_{\setminus k}, \boldsymbol{\varphi})$ and the “missing data” $\gamma_{\setminus k}$. In the CM-steps discussed in Section 2.3, $\boldsymbol{\varphi}$ and $\boldsymbol{\beta}_{\setminus k}$ are restricted to their values from the previous iteration when estimating β_k (Meng and Rubin, 1993). Here, we use an *all-at-once* type optimization where, at iteration t , $(\boldsymbol{\beta}_{\setminus k}, \boldsymbol{\varphi})$ will be fixed to their values at iteration $t - 1$ for all k . The E-step discussed in Section 2.4 updates $E(\mathbf{W}_k)$ and $E(\mathbf{W}_k^2)$, where the expectations are over $\gamma_{\setminus k}$. This E-step estimates \boldsymbol{p} via a plug-in empirical Bayes estimator. After the moments of the \mathbf{W}_k 's are updated, they are used to perform the following CM-steps. The MAP of $\boldsymbol{\omega}$ does not have a closed form. As a result, we perform

the maximization for this parameter via quasi-Newton optimization (Fletcher, 1987). For more discussion contrasting PROBE to other extensions of the EM is available in McLain et al. (2022).

Along with \mathbf{W}_k and $\mathbf{Z}_k = (\mathbf{X}_k \ \mathbf{W}_k)$ described above, we define $\mathbf{W}_0 = \mathbf{X}(\boldsymbol{\gamma}\boldsymbol{\beta})$ and $\mathbf{Z}_0 = (\mathbf{V} \ \mathbf{W}_0)$. The calculations in Section 2.4 require $W_{i0}^{(t-1)} = E(W_{i0}|\boldsymbol{\beta}^{(t-1)}, \mathbf{p}^{(t-1)})$, $W_{ik}^{(t-1)} = E(W_{ik}|\boldsymbol{\beta}_{\setminus k}^{(t-1)}, \mathbf{p}_{\setminus k}^{(t-1)}, \alpha_0^{(t-1)}, \boldsymbol{\omega}^{(t-1)}, \boldsymbol{\varphi}^{(t-1)})$ for $k \geq 1$, and $\mathbf{W}_\ell^{(t-1)} = (W_{1\ell}^{(t-1)}, \dots, W_{n\ell}^{(t-1)})$ for $\ell \in (0, \dots, p)$, with analogous notation for the second moments $W_{i0}^{2(t-1)}$, $W_{ik}^{2(t-1)}$, and $\mathbf{W}_\ell^{2(t-1)}$. Some key quantities in the CM-step updates are $(\mathbf{W}'_\ell \boldsymbol{\Sigma}^{-1})^{(t-1)} = \sum_{i=1}^n W_{i\ell}^{(t-1)} / \sigma_i^{2(t-1)}$ and $(\mathbf{W}'_\ell \boldsymbol{\Sigma}^{-1} \mathbf{W}_\ell)^{(t-1)} = \sum_{i=1}^n W_{i\ell}^{2(t-1)} / \sigma_i^{2(t-1)}$ where $\sigma_i^{2(t-1)} = \exp(-\mathbf{V}_i \boldsymbol{\omega}^{(t-1)})$. Further, let

$$(\mathbf{Z}'_k \boldsymbol{\Sigma}^{-1} \mathbf{Z}_k)^{(t-1)} = \begin{pmatrix} \mathbf{X}'_k \boldsymbol{\Sigma}^{-1(t-1)} \mathbf{X}_k & \mathbf{X}'_k (\boldsymbol{\Sigma}^{-1} \mathbf{W}_k)^{(t-1)} \\ (\mathbf{W}'_k \boldsymbol{\Sigma}^{-1})^{(t-1)} \mathbf{X}_k & (\mathbf{W}'_k \boldsymbol{\Sigma}^{-1} \mathbf{W}_k)^{(t-1)} \end{pmatrix} \quad \text{for } k = 1, \dots, p, \quad (6)$$

and we define $(\mathbf{Z}'_0 \boldsymbol{\Sigma}^{-1} \mathbf{Z}_0)^{(t-1)}$ similarly to (6) where \mathbf{X}_k and \mathbf{W}_k are replaced with \mathbf{V} and \mathbf{W}_0 , respectively.

2.3 CM-step

The CM-steps maximize the expected complete-data log-posterior distribution of $\boldsymbol{\xi}_\ell$ for each partition $\ell \in (0, 1, \dots, p)$. The 0th partition focuses on the parameters $\boldsymbol{\xi}_0 = (\boldsymbol{\varphi}, \alpha_0, \boldsymbol{\omega})$ via $E(\mathbf{Y}|\mathbf{W}_0) = \mathbf{V}\boldsymbol{\varphi} + \alpha_0 \mathbf{W}_0$ and remaining partitions focus on $\boldsymbol{\xi}_k = (\beta_k, \alpha_k)'$ via (5). The complete-data log-posterior distribution is denoted by $l(\boldsymbol{\xi}_\ell|\mathcal{D}, \mathbf{W}_\ell, \boldsymbol{\Gamma}_\ell)$ and is conditional on $\boldsymbol{\Gamma}_\ell$, which represents the hyperparameters for $\boldsymbol{\xi}_\ell$ (Section 2.2). Recall that for $\ell \geq 1$, this corresponds to the log-posterior distribution of $\boldsymbol{\xi}_k$ given $\gamma_k = 1$. The expectation of $l(\boldsymbol{\xi}_\ell|\mathcal{D}, \mathbf{W}_\ell, \boldsymbol{\Gamma}_\ell)$ is conditional on $\boldsymbol{\beta}_{\setminus k}$, $\mathbf{p}_{\setminus k}$, and $\boldsymbol{\xi}_0$ for all $\ell \geq 1$, and on $\boldsymbol{\beta}$ and \mathbf{p} for $\ell = 0$.

At iteration t , the CM-step maximizes

$$\hat{\boldsymbol{\xi}}_\ell^{(t)} = \operatorname{argmax}_{\boldsymbol{\xi}_\ell} E_\ell^{(t-1)} \{l(\boldsymbol{\xi}_\ell | \mathbf{Y}, \mathbf{W}_\ell, \boldsymbol{\Gamma}_\ell)\} \text{ for } \ell = 0, 1, \dots, p, \quad (7)$$

where $E_\ell^{(t-1)}$ represents the expectation given the relevant parameter estimates at iteration $(t-1)$, i.e., given $(\boldsymbol{\beta}, \mathbf{p})$ for $\ell = 0$ and $(\boldsymbol{\beta}_{\setminus \ell}, \mathbf{p}_{\setminus \ell}, \boldsymbol{\xi}_0)$ for $\ell \geq 1$.

For the 0th partition of iteration t , the MAP values for $(\boldsymbol{\varphi}, \alpha_0)$ are

$$\begin{pmatrix} \hat{\boldsymbol{\varphi}}^{(t)} \\ \hat{\alpha}_0^{(t)} \end{pmatrix} = \left\{ (\mathbf{Z}'_0 \boldsymbol{\Sigma}^{-1} \mathbf{Z}_0)^{(t-1)} \right\}^{-1} \left(\mathbf{Z}'_0 \boldsymbol{\Sigma}^{-1} \right)^{(t-1)} \mathbf{Y}. \quad (8)$$

For $\boldsymbol{\omega}^{(t)}$, the MAP has no closed form. As a result, we use a quasi-Newton optimizer (Fletcher, 1987) on the log posterior distribution of $\boldsymbol{\omega}$ in (4) to find the MAP estimate $\boldsymbol{\omega}^{(t)}$. Then, we obtain $\boldsymbol{\Sigma}^{-1(t)} = \exp\{-(\mathbf{V}'\boldsymbol{\omega}^{(t)})\}^{-1}$. For the k th partition of iteration t , the MAP of $\boldsymbol{\xi}_k$ is

$$\hat{\boldsymbol{\xi}}_k^{(t)} = \left\{ (\mathbf{Z}'_k \boldsymbol{\Sigma}^{-1} \mathbf{Z}_k)^{(t-1)} \right\}^{-1} \left(\mathbf{Z}'_k \boldsymbol{\Sigma}^{-1} \right)^{(t-1)} \mathbf{Y}. \quad (9)$$

The E-step used in Section 2.4 requires an estimate of the posterior variance of β_k given $\gamma_k = 1$. Here, the posterior covariance of $\hat{\boldsymbol{\xi}}_k^{(t)}$ is estimated by

$$\left\{ (\mathbf{Z}'_k \boldsymbol{\Sigma}^{-1} \mathbf{Z}_k)^{(t-1)} \right\}^{-1} \left\{ (\mathbf{Z}'_k \boldsymbol{\Sigma}^{-1})^{(t-1)} \mathbf{Z}_k^{(t-1)} \right\} \left\{ (\mathbf{Z}'_k \boldsymbol{\Sigma}^{-1} \mathbf{Z}_k)^{(t-1)} \right\}^{-1}, \quad (10)$$

where $\hat{S}_k^{2(t)}$ denotes the (1,1) element. The posterior variance in (10) accounts for the dependence between \mathbf{X}_k and \mathbf{W}_k . That is, $\hat{S}_k^{2(t)}$ increases as the strength of the dependence between when \mathbf{X}_k and \mathbf{W}_k increases. Recall that in the implementation of our model we split \mathbf{W}_k such that there are separate α parameters for sparse $\mathbf{X}_{\setminus k}(\boldsymbol{\gamma}_{\setminus k} \boldsymbol{\beta}_{\setminus k})$ and non-sparse

$\mathbf{V}\varphi$ components. In this formulation, $\hat{S}_k^{2(t)}$ accounts for the joint dependence between all quantities. This is an important distinction from the posterior variance used in Variational Bayesian approaches to sparse linear regression where the dependence between \mathbf{X}_k and the other components is ignored (Carbonetto and Stephens, 2012). We use the $\hat{S}_k^{2(t)}$'s in Section 2.6 to create prediction intervals.

2.4 E-step

The E-step described in this Section performs updates for β_k and p_k . To accelerate convergence, we limit the step size using learning rates $q^{(t)}$ via

$$\beta_k^{(t)} = (1 - q^{(t)})\beta_k^{(t-1)} + q^{(t)}\hat{\beta}_k^{(t)}, \text{ and } S_k^{2(t)} = \{(1 - q^{(t)})(S_k^{2(t-1)})^{-1} + q^{(t)}(\hat{S}_k^{2(t)})^{-1}\}^{-1}. \quad (11)$$

A learning rate $q^{(t)} = 1$ indicates no contribution from the previous iteration estimates, whereas $q^{(t)} = 0$ ignores the current estimate. We use $q^{(t)} = \frac{1}{t+1}$, which creates a moving average of β_k over iterations. Varadhan and Roland (2008), Vehtari et al. (2020), and Minka and Lafferty (2002) provide a discussion on learning rates and their implications. In our approach, the learning rate helps accelerate the ECM algorithm and prevents oscillations between estimates (Sutskever et al., 2013; McLain et al., 2022).

In Bayesian frameworks, estimation of $p_k = P(\gamma_k = 1 | \mathbf{Y}, \pi_0)$ is commonly done using Bayes factors based on the marginal likelihood given $\gamma_k = 0$ and $\gamma_k = 1$. However, increasingly uninformative priors force Bayes factors towards the null (i.e., *Barlett's paradox*, see Liang et al., 2008). To mitigate this and maintain uninformative priors, we use a plug-in empirical Bayes estimator of p_k , which is motivated by two-group testing scenarios where many test statistics with zero and non-zero expectations are available (Castillo and Roquain, 2020; Efron, 2008; Liang et al., 2008, among others). We define test statistics as

$\mathcal{T}_k^{(t)} = \beta_k^{(t)} / S_k^{(t)}$ with distribution $(1 - \gamma_k)f_{\mathcal{Z}}(\cdot) + \gamma_k f_1(\cdot)$, where $f_{\mathcal{Z}}(\cdot) \sim N(0, 1)$ and f_1 is unknown and based on f_{β} . We also require π_0 , a proportion of null hypotheses, so that the estimator is conditional on an observed value of test statistics with an expectation of zero. This yields empirical Bayes estimates of the posterior distribution of $p_k^{(t)}$ via

$$p_k^{(t)} = 1 - \frac{\hat{\pi}_0^{(t)} f_0(\mathcal{T}_k^{(t)})}{\hat{f}^{(t)}(\mathcal{T}_k^{(t)})}. \quad (12)$$

The estimator in (12) sets $\hat{\pi}^{(t)} = \sum_k I(P_k^{(t)} \geq \lambda) / \{p \times (1 - \lambda)\}$, based on Storey (2007), where $P_k^{(t)}$ is a two-sided p-value for $\mathcal{T}_k^{(t)}$ and $\lambda = 0.1$ (Blanchard and Roquain, 2009). We use Gaussian kernel density estimation on $\mathcal{T}^{(t)} = (\mathcal{T}_1^{(t)}, \dots, \mathcal{T}_p^{(t)})$ to obtain $\hat{f}^{(t)}$ (Silverman, 1986).

Finally, we estimate the first and second moments of \mathbf{W}_{ℓ} . These moments are expectations of \mathbf{W}_{ℓ} over the unknown γ . Through the use of the ECM, the values of β are fixed at their estimates from the previous iteration. Independence between γ_k 's allows effective computation to be performed at the observation i level through

$$W_{i0}^{(t)} = E\{\mathbf{X}_i(\gamma\beta) | \beta^{(t)}, \mathbf{p}^{(t)}\} = \mathbf{X}_i(\beta^{(t)} \mathbf{p}^{(t)}), \quad (13)$$

and $W_{i0}^{2(t)} = E(W_{i0}^2 | \beta^{(t)}, \mathbf{p}^{(t)}) = \text{Var}(W_{i0} | \beta^{(t)}, \mathbf{p}^{(t)}) + (W_{i0}^{(t)})^2$ where

$$\text{Var}(W_{i0} | \beta^{(t)}, \mathbf{p}^{(t)}) = \mathbf{X}_i^2 \left\{ \beta^{(t)2} \mathbf{p}^{(t)} (1 - \mathbf{p}^{(t)}) \right\}. \quad (14)$$

Online calculations of $\mathbf{W}_k^{(t)}$ and $\mathbf{W}_k^{2(t)}$ are made by subtracting the contributions of the k th predictor from $\mathbf{W}_0^{(t)}$ and $\mathbf{W}_0^{2(t)}$, respectively. As a result, the high-dimensional matrix computations in (13) and (14) only need to be made once per iteration.

2.5 Full algorithm and model checks

The H-PROBE method converges when subsequent changes in $\mathbf{W}_0^{(t)}$ are small since $\mathbf{W}_0^{(t)}$ captures the trajectory of all model parameters. Specifically, convergence at iteration t is quantified via $CC^{(t)} = \log(n) \max_i \left\{ (W_{i0}^{(t)} - W_{i0}^{(t-1)})^2 / \text{Var}(W_{i0} | \boldsymbol{\beta}^{(t)}, \mathbf{p}^{(t)}) \right\}$, where the ECM algorithm has converged when $CC^{(t)} < \chi_{1,0.1}^2$ and $\chi_{1,0.1}^2$ represents the 0.1th quantile of a χ^2 distribution with 1 degree of freedom. Here, $\log(n)$ controls for the impact of sample size on the maximum of $\chi_{1,0.1}^2$ (Embrechts et al., 2013). We initiate the algorithm using $\boldsymbol{\beta}^{(0)} = \mathbf{0}$ and $\mathbf{p}^{(0)} = \mathbf{0}$, which gives $\mathbf{W}^{(0)} = \mathbf{0}$ and $\mathbf{W}^{2(0)} = \mathbf{0}$. For the elements of $\boldsymbol{\omega}^{(0)}$, we initialize the first element to $\log(s_Y^2)$, where s_Y^2 is the sample variance of \mathbf{Y} , and all remaining elements to 0. These initial values lead to estimates of $\hat{\beta}_k^{(1)}$ that correspond to the coefficient of a simple linear regression for each \mathbf{X}_k on \mathbf{Y} .

Algorithm 1 shows H-PROBE steps in sequence. Upon convergence, H-PROBE provides MAP estimates $\tilde{\boldsymbol{\beta}}$, $\tilde{\mathbf{p}}$, $\tilde{\boldsymbol{\varphi}}$, $\tilde{\alpha}_0$, $\tilde{\boldsymbol{\omega}}$, $\tilde{\boldsymbol{\Sigma}}$ as well as \tilde{S}_k^2 , the posterior variance of $\tilde{\beta}_k | \gamma_k = 1$, for all k . In Simulations (Section 3) and Data Analysis (Section 4), we use $\tilde{\alpha}_0(\tilde{\mathbf{p}}\tilde{\boldsymbol{\beta}})$ – a combination of $E(\boldsymbol{\gamma}\boldsymbol{\beta})$ assuming a normal posterior and the MAP of α_0 – to estimate $\boldsymbol{\gamma}\boldsymbol{\beta}$. While the properties of $\boldsymbol{\varphi}$ are not the focus of this research, we do wish to account for the uncertainty it contributes to the MAP estimates in the prediction intervals constructed below. To this end, let $\tilde{\Psi} = \{(\mathbf{Z}'_0 \tilde{\boldsymbol{\Sigma}}^{-1} \mathbf{Z}_0)^{(t-1)}\}^{-1} \{(\mathbf{Z}'_0 \tilde{\boldsymbol{\Sigma}}^{-1})^{(t-1)} \mathbf{Z}_0^{(t-1)}\} \{(\mathbf{Z}'_0 \tilde{\boldsymbol{\Sigma}}^{-1} \mathbf{Z}_0)^{(t-1)}\}^{-1}$ denote the estimated posterior covariance of $(\tilde{\boldsymbol{\varphi}}, \tilde{\alpha}_0)$.

The residuals from a high-dimensional homoscedastic regression model can be used to identify variables that may have an association with the residual variance and appropriate forms of such variables such that the parametric assumptions of the variance model in (3) are adequately met. Levene's, Barlett's, or Brown-Forsythe are tests that can be used to assess if the variance of the residuals is related to a candidate heterogeneity variable (Seber

Algorithm 1 The H-PROBE algorithm

Initialize $\mathbf{W}^{(0)}$, $\mathbf{W}^{2(0)}$, and $\Sigma^{(0)}$ **while** $CC^{(t)} \geq \chi_{1,\varepsilon}^2$ and $\max(\mathbf{p}^{(t)}) > 0$ **do****CM-step**Use $\mathbf{W}_\ell^{(t-1)}$ and $\mathbf{W}_\ell^{2(t-1)}$ to estimate $\boldsymbol{\xi}_\ell^{(t)}$ for $\ell = 0, 1, \dots, p$ via (8)-(9).**E-step**(a) Calculate $\beta_k^{(t)}$ and $S_k^{2(t)}$ using (11) for all k .(b) Estimate $\hat{f}^{(t)}$ and $\hat{\pi}_0^{(t)}$ and use them to calculate $\mathbf{p}^{(t)}$ via (12).(c) Calculate $\mathbf{W}^{(t)}$ and $\mathbf{W}^{2(t)}$ via (13) and (14).Calculate $CC^{(t)}$ and check convergence.

and Lee, 2003). Further, plots of the residuals or the log-squared residuals can be used to determine if transformations of variables are necessary. Figure 1 shows an example of residual plots used to validate model assumptions. Both panels are from homoscedastic LASSO models with 50 observations of 100 sparse predictors. The data used in each model was generated such that the residual variance is associated with a linear covariate (Panel (a)) and a non-linear covariate ($variable + variable^2$, Panel (b)). In both plots, the covariate has a relationship with the residual variance. This association is weaker in Panel (a), while it is stronger in Panel (b). The residuals in Panel (a) show that the linear form of the heterogeneity variable fulfills the parametric assumptions of the variance model in (3), whereas Panel (b) shows that additional non-linear transformations of the heterogeneity variable are needed to fulfill the assumptions of the variance model.

2.6 Prediction intervals

This research aims to develop point estimates and prediction intervals for a future observation not included in the training set with predictor data \mathbf{X}_l and \mathbf{V}_l . MAP estimation does not provide posterior distributions of model parameters, just their mode, limiting predictive inference capabilities. As a result, we assume that the estimates of the posterior variance of $\boldsymbol{\varphi}$ and $\tilde{\beta}_k | \gamma_k = 1$ for all k can be used to capture the posterior variability of

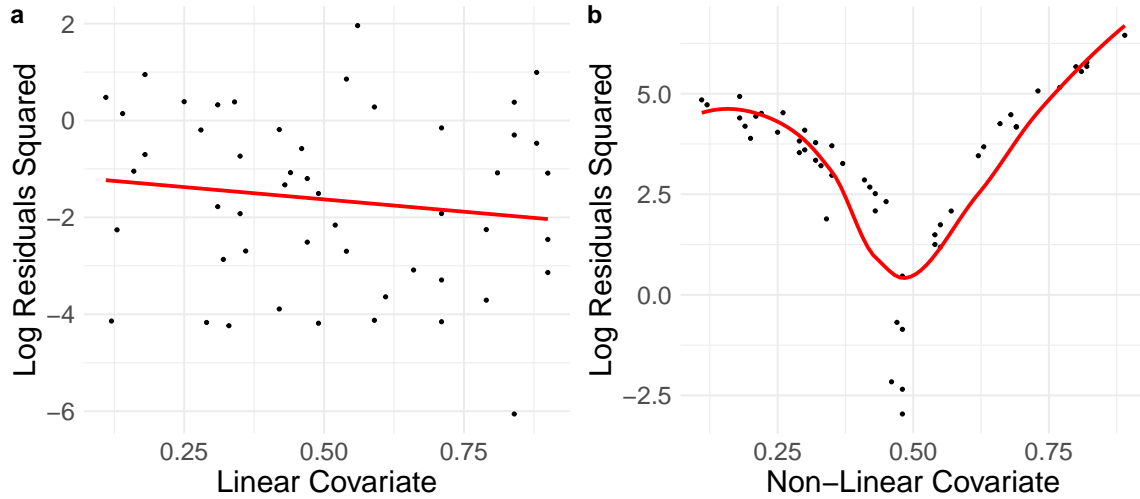


Figure 1: Log Residuals Squared for homoscedastic LASSO models plotted against a linear and non-linear heterogeneity variable.

these parameters. To predict for a new observation we use the MAP of the predicted value $\tilde{Y}_l = \mathbf{V}_l \tilde{\boldsymbol{\varphi}} + \tilde{W}_{l0} \tilde{\alpha}_0$ where \tilde{W}_{l0} is obtained by plugging in \mathbf{X}_l and the MAP estimates into (13). Further, the variance of \tilde{W}_{l0} is estimated with

$$\tilde{\nu}_{l0} = \mathbf{X}_l^2 \left\{ \tilde{\boldsymbol{p}} \tilde{\boldsymbol{S}}^2 + \tilde{\boldsymbol{\beta}}^2 \tilde{\boldsymbol{p}}(1 - \tilde{\boldsymbol{p}}) \right\}.$$

To estimate the variance of the expectation of \tilde{Y}_l while acknowledging the uncertainty in \tilde{W}_{l0} , we use

$$\text{Var}(\tilde{Y}_l) = \mathbf{Z}'_{0l} \tilde{\Psi} \mathbf{Z}_{0l} + \tilde{\nu}_{l0} \{ \text{Var}(\alpha_0) + \tilde{\alpha}_0^2 \},$$

where $\mathbf{Z}_{0l} = (\mathbf{V}_l, \tilde{W}_{l0})'$ and $\text{Var}(\alpha_0)$ is the last diagonal element of $\tilde{\Psi}$, which is motivated by the measurement error literature (Buonaccorsi, 1995). Prediction intervals (PIs) can be formed using the appropriate critical values with $\text{Var}(\tilde{Y}_l) + \tilde{\sigma}_l^2$ where $\tilde{\sigma}_l^2 = \exp\{-(\mathbf{V}'_l \tilde{\boldsymbol{\omega}})\}$ denotes the MAP estimate of the variance for subject l . In the following sections, we evaluate the empirical coverage probabilities of PIs using this approach for test data via simulation studies and a clinical application.

3 Numerical Studies

We perform numerical studies to evaluate the performance of H-PROBE. We generate the outcome using $Y_i = \mathbf{X}'_i(\boldsymbol{\gamma}\boldsymbol{\beta}) + \epsilon_i$, where $\epsilon_i \sim N(0, \sigma_i^2)$, $\sigma_i^2 = \exp(\mathbf{V}'_i\boldsymbol{\omega})$, $\boldsymbol{\beta} \sim U(0, 2\eta_\beta)$, and $\boldsymbol{\omega}$ is set based on the signal-to-noise ratio (SNR). Specifically, $\omega_j = \omega_0$ for all j where ω_0 is such that $SNR = E\{Var(\mathbf{X}'_i\boldsymbol{\gamma}\boldsymbol{\beta})\}/E(\sigma_i^2)$ with $SNR = 1$, or 2. We used a Gaussian random field (GRF , Schlather et al., 2015) to generate \mathbf{X} and $\boldsymbol{\gamma}$. Let $L_s(\mathbf{d}_k) \sim GRF(\mathbf{0}, \Sigma_s)$, where the variance Σ_s follows a squared exponential function defined as $\Sigma_s = \exp\{-\|(\mathbf{d}_k - \mathbf{d}_{k'})/s\|_2^2\}$ and $s = 20$. In the GRF , $\mathbf{d}_k = (d_{1k}, d_{2k})$ represents the coordinates of predictor \mathbf{X}_k on the $\sqrt{p} \times \sqrt{p}$ grid. $\boldsymbol{\gamma}$ was generated such that $\gamma_k = \mathbf{1}\{L_{20}(\mathbf{d}_k) < Q_\pi\}$ where Q_π is a value ensuring $|\boldsymbol{\gamma}|/p = \pi$. Continuous and binary predictors \mathbf{X} were generated using $X_{ik} = L_{is}(\mathbf{d}) + a_i$ and $X_{ik} = I\{L_{is}(\mathbf{d}) + a_i < 0\}$, respectively, where $a_i \sim N(0, \frac{3}{4})$. \mathbf{V} included an intercept along with half standard normal and half Bernoulli(0.5) predictors.

Simulation settings were varied by the number of predictors in \mathbf{X} , $p = (20^2, 75^2)$, the number of predictors in \mathbf{V} including an intercept, $v = (3, 7)$, the proportion of non-zero coefficients, $\pi = (0.01, 0.05)$, the signal-to-noise ratio, $SNR = (1, 2)$, and the average effect size of $\boldsymbol{\beta}$, $\eta_\beta = (0.3, 0.8)$. For brevity, we focus below on the results for $\eta_\beta = 0.8$ and binary \mathbf{X} predictors; results for $\eta_\beta = 0.3$ and continuous \mathbf{X} were overwhelmingly similar and are omitted. All simulations had $N = 400$ observations and were repeated 400 iterations. We compare H-PROBE to PROBE and LASSO. For LASSO, we used the `glmnet` R package to implement ten-fold cross-validation (CV) to select parameters requiring tuning. We considered comparisons with Daye et al. (2012), but the computation requirements were prohibitive, with many settings running for over one hour per iteration.

We compared the performance of the methods with Root Mean Squared Error (RMSE) and Median Absolute Deviation (MAD, in Supplemental Materials Section A) of $\mathbf{X}'(\boldsymbol{\gamma}\boldsymbol{\beta})$,

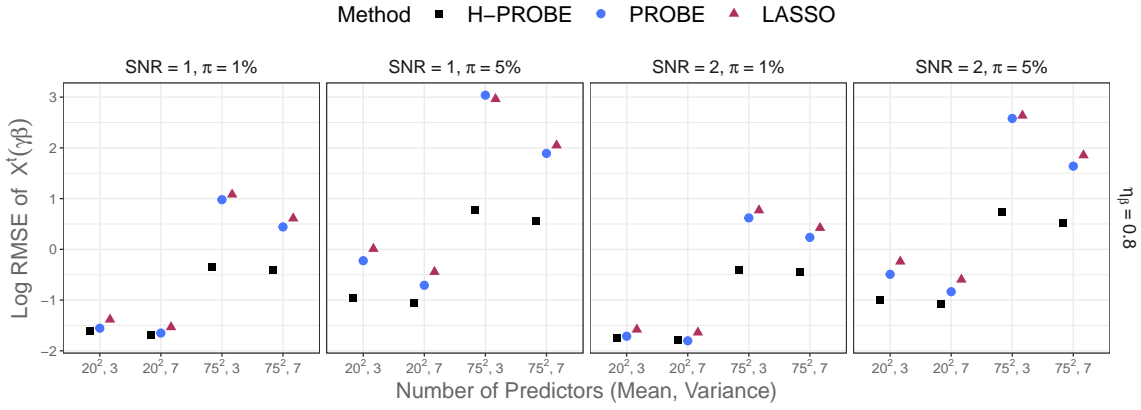


Figure 2: Log Root Mean Squared Errors (RMSE) of $\mathbf{X}'(\gamma\boldsymbol{\beta})$ for H-PROBE (black squares), PROBE (blue circles), or LASSO (maroon triangles), for selected simulation settings.

where data \mathbf{X} consists of new observations not used during estimation (test set). Figures 2 and A.1 show that for all simulation settings except one, H-PROBE had the lowest RMSE and MAD. H-PROBE led to marked efficiency gains when the proportion of signals, the number of predictors on the mean, or the effect size of $\boldsymbol{\beta}$ were higher.

For H-PROBE and PROBE, we also obtained empirical coverage probabilities (ECPs) of 95% prediction intervals (PIs), which we estimated as the proportion of PIs that contained $Y_{i,test}$. Figure 3 shows that the average ECP for H-PROBE PIs consistently remains centered at 0.95, whereas the average ECP for PROBE PIs exceeds 0.95 and has interquartile ranges that do not cover the 0.95 level, particularly when $p = 75^2$. Supplemental Material Figure A.2 shows (log) PI lengths associated with the PI ECPs in Figure 3.

To compare the variable selection abilities of the methods, we calculated True Positive Rate (TPR) $TPR = \sum_{k;\hat{\gamma}_k=1} \hat{\gamma}_k / |\boldsymbol{\gamma}|$ and the False Discovery Rate (FDR) $FDR = \sum_{k;\hat{\gamma}_k=0} \hat{\gamma}_k / |\hat{\boldsymbol{\gamma}}|$ where $\hat{\gamma}_k = 1$ if variable k was ‘selected’ for the given method. For H-PROBE and PROBE $\hat{\gamma}_k = I(p_k > 0.5)$, a predictor was selected for LASSO if the estimated coefficient was non-zero. H-PROBE performed well in variable selection. Figure 4a shows that H-PROBE correctly selects the highest proportion of the true signals in all settings.

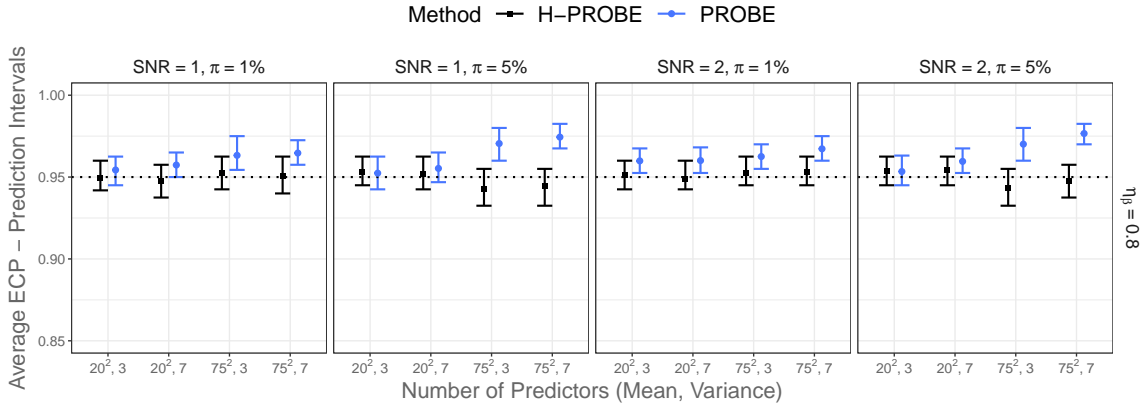


Figure 3: Empirical Coverage Probabilities (ECPs) of Prediction Intervals (PIs) for $Y_{i,test}$ for H-PROBE (black squares) and PROBE (blue circles), for selected simulation settings. Vertical lines represent the first and third quartiles of the distributions of ECPs for PIs.

This is strongly emphasized when the number of true signals ($|\gamma|$) was 281 with $p = 75^2$, and performance is closer between methods when there are only 4 signals. In Figure 4b, H-PROBE has a lower FDR than LASSO in all settings. Comparing the FDR between PROBE and H-PROBE, we see they are similar for $p = 20^2$ and lower for PROBE when $p = 75^2$ (where PROBE is markedly conservative).

4 Data Analysis

We return to our motivating example to illustrate the use and distinctive features of the H-PROBE method. This application aims to use patients’ imaging and brain damage data to predict the Aphasia Quotient (AQ) score, which in turn guides post-stroke aphasia treatment decisions. The data include $n = 167$ patients who have recently experienced a left-hemispheric stroke and are candidates for language rehabilitation therapy (Johnson et al., 2019; Yourganov et al., 2015). All individuals were scanned using a 3T MRI scanner, and an expert identified the lesion boundaries by hand via a high-resolution T2 scan. The lesions were then coregistered to the individual’s T1 scan and warped to have a common

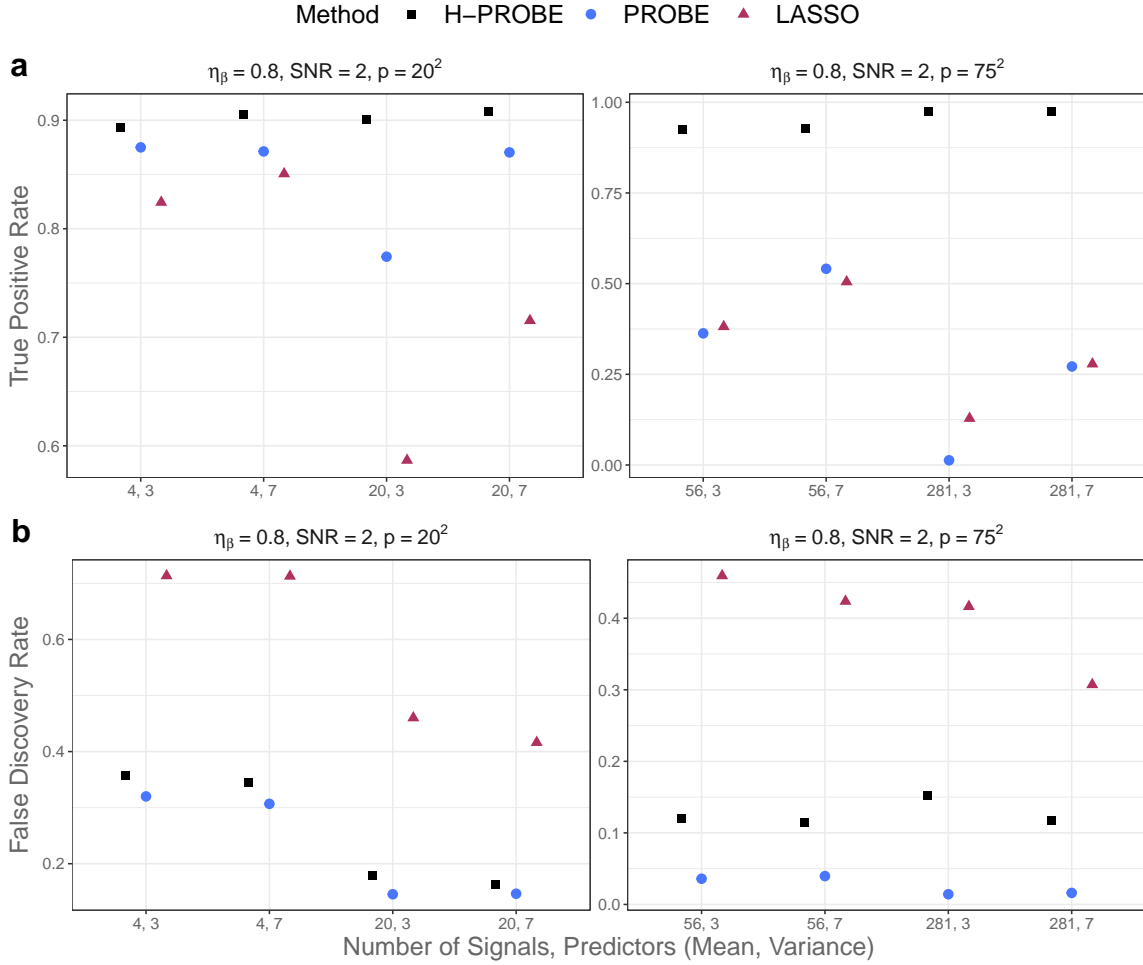


Figure 4: True Positive Rate and False Discovery Rate for H-PROBE (black squares), PROBE (blue circles), or LASSO (maroon triangles), for selected simulation settings.

size and shape through an enantiomorphic normalization clinical toolbox (Nachev et al., 2008; Rorden et al., 2012). The resulting data contain over 5×10^5 binary features capturing the presence or absence of lesions in each 1 mm^3 brain voxel.

Before comparing the performance of heteroscedastic and homoscedastic approaches in this clinical scenario, we streamlined the analysis by performing a marginal screening procedure based on Wang and Leng (2016) and retained 3×10^4 candidate imaging predictors. Total Brain Damage (TBD) was retained, i.e., the total number of voxels with lesions in the brain (out of 5×10^5). The outcome of interest is the AQ, a measure of language ability.

In Figure 5a the relationship between AQ and TBD is displayed. Most AQ values are

concentrated near the top of the range for lower brain damage and diffuse as brain damage increases. The residuals (squared and log-transformed) from homoscedastic PROBE by TBD are shown in Figure 5b. There is a strong non-linear relationship between the error variance and TBD. Transformations of AQ also show evidence heterogeneity (see Figure B.5 and transformation details in Supplementary Material Section B). As a result, we analyze AQ on the original scale and account for heteroscedasticity in this application. We use the H-PROBE approach, where the model on the variance includes TBD as well as its square-root transformation as predictors

$$\Sigma = \text{diag}(\exp \left\{ - \left(\omega_1 \mathbf{1} + \omega_2 \times \text{TBD} + \omega_3 \times \sqrt{\text{TBD}} \right) \right\}.$$

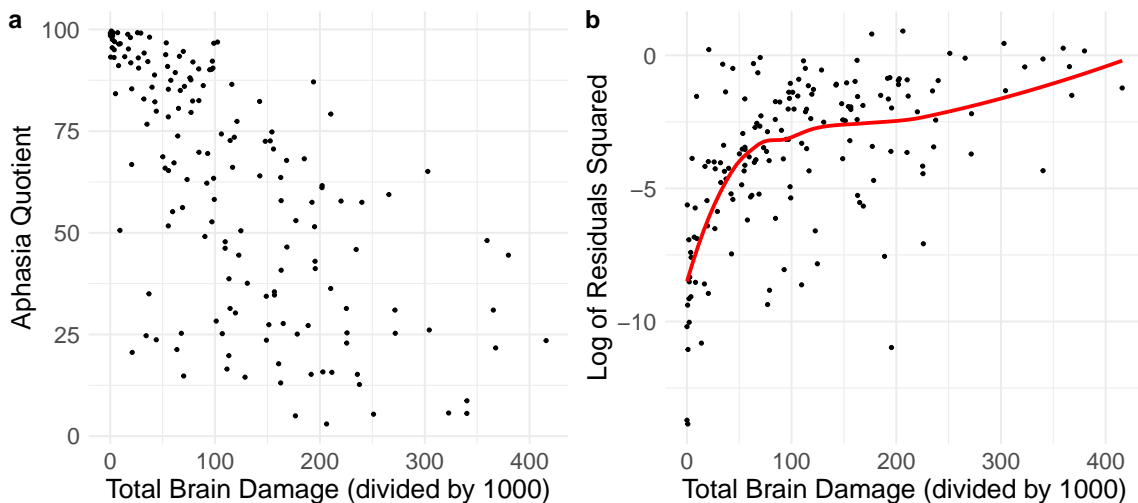


Figure 5: (a) Aphasia Quotient (AQ) outcome by total brain damage (defined as the number of brain voxels with lesions). The mean (median) AQ is 62.1 (66.8) with a standard deviation of 29.4, and range 3.0–99.6. (b) Log Residuals Squares from PROBE using candidate brain images as predictors.

Our analyses include Conformal Inference based on LASSO (*split* variant, Tibshirani and Foygel, 2019), PROBE, and a Bayesian method based on empirical priors for prediction in sparse high-dimensional linear regression (EBREG, Martin and Tang, 2020). EBREG provides a simple algorithm based on a local search improvement rule that correctly identi-

fies the support of the regression coefficients and subsequently provides prediction intervals. We used R packages `probe`, `conformalInference`, and `ebreg` with 5-fold CV and default parameters (Tang and Martin, 2021; Tibshirani and Foygel, 2019; McLain and Zgodic, 2021). For all methods, we modeled the mean of AQ (\mathbf{Y}) using the 3×10^4 candidate imaging predictors (\mathbf{X}), $\mathbf{Y} = \beta\mathbf{X} + \mathbf{e}$.

To evaluate and compare the methods, we used 5-fold CV to calculate Mean Squared Predictive Error (MSPE), Median Absolute Deviation (MAD), and empirical coverage probability (ECP) of 95% PIs where coverage implies that the PI for a given *test* subject included the actual observation. Figures in Supplemental Materials Section B provide additional analysis results, including per-voxel statistical brain maps that compare H-PROBE to PROBE.

Method \ Metric	MAD	MSPE	Average PI Length	ECP
H-PROBE	8.635	220.671	60.749	0.952
PROBE	11.929	380.673	71.558	0.922
Conformal Inference	13.393	509.903	100.192	0.946
EBREG	17.677	614.314	91.582	0.940

Table 1: Performance metrics for H-PROBE and three comparison methods, PROBE, Conformal Inference, and EBREG, for the brain study analysis.

Table 1 shows that H-PROBE had the lowest MAD and MSPE, followed by PROBE, Conformal Inference, and EBREG. H-PROBE also had the shortest average PI length with ECP close to the nominal 0.95 level. This pattern is consistent with H-PROBE providing accurate predictions for new observations and down-weighting observations with high estimated variance. Figure 6 shows PI lengths for observations for each method by fold. The Conformal Split and EBREG methods had similar PI lengths. As anticipated, H-PROBE displayed the widest range of PI lengths, reflected by the differing estimated $\tilde{\sigma}_i^2$

by observation (see Figure B.6 in Supplementary Material Section B). While H-PROBE had the lowest average PI length across observations it had the largest ECP, so the narrower PI's do not sacrifice coverage. The PI lengths also differed by prediction.

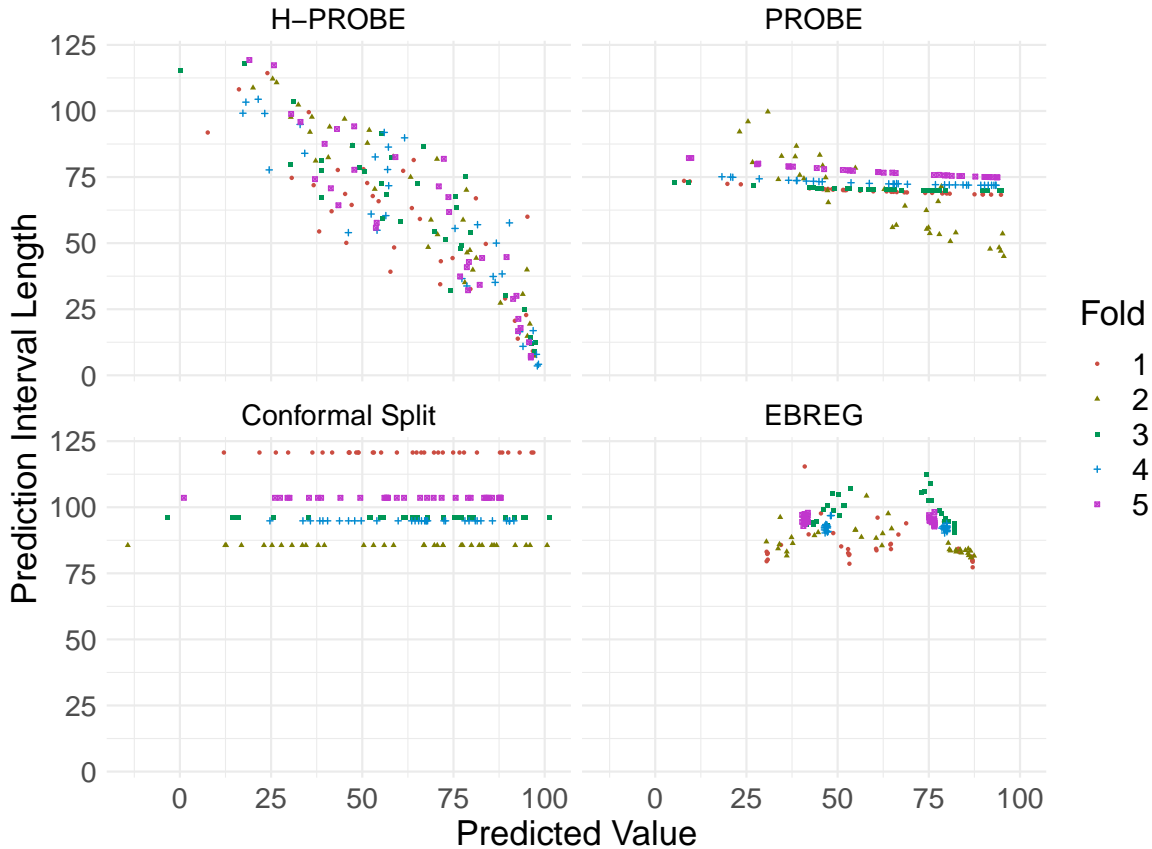


Figure 6: Prediction interval lengths by predicted values using H-PROBE and three comparison methods, PROBE, Conformal Inference, and EBREG. The color legend represents the cross-validation fold in which predictions were obtained.

5 Discussion

In this paper, we developed a novel approach that leverages MLG distribution theory to conduct high-dimensional linear regression for heteroscedastic data. H-PROBE uses a Bayesian framework with parameter expansion and minimally informative priors on the parameters. H-PROBE is a computationally effective solution to sparse linear regression in

heteroscedastic settings that combines an empirical Bayes estimator with the PX-ECM algorithm. Simulation studies illustrated that accounting for heterogeneity in variance errors via the H-PROBE method generally resulted in more accurate estimation and prediction, as shown by lower MSEs and MADs for model predictions, compared to the PROBE and LASSO approaches. Empirical coverage probabilities of prediction intervals reached and stayed at the nominal 95% level, with tighter prediction interval lengths than other methods. H-PROBE is the first Bayesian approach to address these issues in high-dimensional settings.

We focused our research on the situation where known markers of heterogeneity exist in the data. However, in practice, the variables' impact heterogeneity may be unknown. A worthy extension of H-PROBE is to the situation where model selection on mean and variance parameters is required (e.g., Chiou et al., 2020; Zhou et al., 2021). If the heterogeneity markers are appropriately included in the variance model, observations with high residual variability will be accordingly down-weighted. This is opposed to situations where trimming observations from the analysis may be desired (Yang et al., 2018; Filzmoser and Nordhausen, 2021), e.g., this commonly occurs in meta-analyses (Shi and Lin, 2019). The development of Bayesian high-dimensional variable selection methods that trim – and possibly incorporate variables related to trimming (e.g., study sample size) – is another worthy avenue of future research.

Our analyses further reinforced that appropriately accounting for non-constant error variances can lead to improvements in predictive ability and prediction interval lengths while maintaining coverage. This has important clinical implications. When using markers such as predicted AQ to formulate treatment plans for post-stroke aphasia, not only is prediction accuracy important but also prediction uncertainty (PIs and ECP). This allows

clinicians to define treatment courses that weigh a range of potential treatment outcomes a patient may experience based on the PIs of the predicted AQ. PIs and PI lengths that capture patient-level heteroscedasticity enable personalized treatment decisions based on each patient’s stroke-induced total brain damage and MRI imaging. In this application, homoscedastic methods such as Conformal Inference, PROBE, and EBREG are likely to lead to less accurate predicted AQ and, thus, suboptimal treatment decisions compared to H-PROBE.

References

- Alfons, A., Croux, C., and Gelper, S. (2013), “Sparse least trimmed squares regression for analyzing high-dimensional large data sets,” *The Annals of Applied Statistics*, 7, 226–248.
- Belloni, A., Chernozhukov, V., and Wang, L. (2014), “Pivotal Estimation via Square-Root LASSO in Nonparametric Regression,” *The Annals of Statistics*, 42, 757–788.
- Blanchard, G. and Roquain, E. (2009), “Adaptive FDR control under independence and dependence,” *Journal of Machine Learning Research*, 10, 2837–2831.
- Bradley, J., Holan, S., and Wikle, C. (2020), “Bayesian Hierarchical Models With Conjugate Full-Conditional Distributions for Dependent Data From the Natural Exponential Family,” *Journal of the American Statistical Association*, 115, 2037–2052.
- Buonaccorsi, J. P. (1995), “Prediction in the presence of measurement error: General discussion and an example predicting defoliation,” *Biometrics*, 1562–1569.
- Carbonetto, P. and Stephens, M. (2012), “Scalable Variational Inference for Bayesian Vari-

- able Selection in Regression, and Its Accuracy in Genetic Association Studies,” *Bayesian Analysis*, 7, 73–108, publisher: International Society for Bayesian Analysis.
- Carroll, R. (1988), *Transformation and weighting in regression*, New York: Chapman and Hall.
- Carroll, R. J. and Ruppert, D. (1988), *Transformation and weighting in regression*, vol. 30, CRC Press.
- Castillo, I. and Roquain, É. (2020), “On spike and slab empirical Bayes multiple testing,” *The Annals of Statistics*, 48, 2548–2574.
- Chiou, H. T., Guo, M., and Ing, C. K. (2020), “Variable selection for high-dimensional regression models with time series and heteroscedastic errors,” *Journal of Econometrics*, 216, 118–136.
- Cleveland, W. (1993), *Visualizing Data*, Hobart Press.
- Daye, Z. J., Chen, J., and Li, H. (2012), “High-Dimensional Heteroscedastic Regression with an Application to eQTL Data Analysis,” *Biometrics*, 68, 316–326.
- Efron, B. (2008), “Microarrays, Empirical Bayes and the Two-Group Model,” *Statistical Science*, 23, 1–22.
- Efron, B., Tibshirani, R., Storey, J. D., and Tusher, V. (2001), “Empirical Bayes analysis of a microarray experiment,” *Journal of the American Statistical Association*, 96, 1151–1160.
- Embrechts, P., Klüppelberg, C., and Mikosch, T. (2013), *Modelling extremal events: for insurance and finance*, vol. 33, Springer Science & Business Media.

- Filzmoser, P. and Nordhausen, K. (2021), “Robust linear regression for high-dimensional data: An overview,” *Wiley Interdisciplinary Reviews: Computational Statistics*, 13, 1–18.
- Fletcher, R. (1987), *Practical Methods of Optimization*, New York: John Wiley & Sons.
- Johnson, L., Basilakos, A., Yourganov, G., Cai, B., Bonilha, L., Rorden, C., and Fridriksson, J. (2019), “Progression of Aphasia Severity in the Chronic Stages of Stroke,” *American Journal of Speech-Language Pathology*, 28, 639–649.
- Lei, J., G’Sell, M., Rinaldo, A., Tibshirani, R. J., and Wasserman, L. (2018), “Distribution-free predictive inference for regression,” *Journal of the American Statistical Association*, 113, 1094–1111.
- Liang, F., Paulo, R., Molina, G., Clyde, M. A., and Berger, J. O. (2008), “Mixtures of g priors for Bayesian variable selection,” *Journal of the American Statistical Association*, 103, 410–423.
- Liu, C., Rubin, D. B., and Wu, Y. N. (1998), “Parameter expansion to accelerate EM: The PX-EM algorithm,” *Biometrika*, 85, 755–770.
- Martin, R. and Tang, Y. (2020), “Empirical Priors for Prediction in Sparse High-dimensional Linear Regression.” *Journal of Machine Learning Research*, 21, 1–30.
- McLain, A. C. and Zgodic, A. (2021), “Fitting high-dimensional linear regression models with probe,” <https://github.com/alexmcclain/UNHIDEM>.
- McLain, A. C., Zgodic, A., and Bondell, H. (2022), “Sparse high-dimensional linear regression with a partitioned empirical Bayes ECM algorithm.” <https://arxiv.org/abs/2209.08139>.

- Meng, X. L. and Rubin, D. B. (1993), “Maximum likelihood estimation via the ECM algorithm: A general framework,” *Biometrika*, 80, 267–278.
- Minka, T. and Lafferty, J. (2002), “Expectation-propagation for the generative aspect model,” in *Proceedings of the Eighteenth conference on Uncertainty in artificial intelligence*, pp. 352–359.
- Nachev, P., Coulthard, E., Jäger, H. R., Kennard, C., and Husain, M. (2008), “Enantiomorphic normalization of focally lesioned brains,” *Neuroimage*, 39, 1215–1226.
- Odekar, A. and Hallowell, B. (2005), “Comparison of Alternatives to Multidimensional Scoring in the Assessment of Language Comprehension in Aphasia,” *American Journal of Speech-Language Pathology*, 14, 337–345.
- Parker, P., Holan, S., and Wills, S. (2021), “A general Bayesian model for heteroskedastic data with fully conjugate full-conditional distributions,” *Journal of Statistical Computation and Simulation*, 91, 3207–3227.
- Ray, K. and Szabó, B. (2021), “Variational Bayes for High-Dimensional Linear Regression With Sparse Priors,” *Journal of the American Statistical Association*, 0, 1–12.
- Risser, A. H. and Spreen, O. (1985), “The western aphasia battery,” *Journal of clinical and experimental neuropsychology*, 7, 463–470.
- Rorden, C., Bonilha, L., Fridriksson, J., Bender, B., and Karnath, H.-O. (2012), “Age-specific CT and MRI templates for spatial normalization,” *Neuroimage*, 61, 957–965.
- Rousseeuw, P. (1984), “Least median of squares regression,” *Journal of the American Statistical Association*, 79, 871–880.

- Rousseeuw, P. and Van Driessen, K. (2006), “Computing LTS regression for large data sets,” *Data Mining and Knowledge Discovery*, 12, 29–45.
- Schlather, M., Malinowski, A., Menck, P. J., Oesting, M., and Storkorb, K. (2015), “Analysis, Simulation and Prediction of Multivariate Random Fields with Package RandomFields,” *Journal of Statistical Software*, 63, 1–25.
- Seber, G. A. and Lee, A. J. (2003), *Linear regression analysis*, vol. 330, John Wiley & Sons.
- Shi, L. and Lin, L. (2019), “The trim-and-fill method for publication bias: practical guidelines and recommendations based on a large database of meta-analyses,” *Medicine*, 98.
- Silverman, B. W. (1986), *Density estimation for statistics and data analysis*, Monographs on Statistics and Applied Probability, Chapman & Hall, London.
- Storey, J. D. (2007), “The optimal discovery procedure: a new approach to simultaneous significance testing,” *Journal of the Royal Statistical Society: Series B (Methodological)*, 69, 347–368.
- Sutskever, I., Martens, J., Dahl, G., and Hinton, G. (2013), “On the importance of initialization and momentum in deep learning,” in *International conference on machine learning*, PMLR, pp. 1139–1147.
- Tang, Y. and Martin, R. (2021), *ebreg: Implementation of the Empirical Bayes Method*, r package version 0.1.3.
- Temlyakov, V. (2000), “Weak greedy algorithms,” *Advances in Computational Mathematics*, 12, 213–227.
- Tibshirani, R. and Foygel, R. (2019), “Conformal prediction under covariate shift.” *Advances in neural information processing systems*.

- Varadhan, R. and Roland, C. (2008), “Simple and Globally Convergent Methods for Accelerating the Convergence of Any EM Algorithm.” *Scandinavian Journal of Statistics*, 35, 335–353.
- Vehtari, A., Gelman, A., Sivula, T., Jylänki, P., Tran, D., Sahai, S., Blomstedt, P., Cunningham, J. P., Schiminovich, D., and Robert, C. P. (2020), “Expectation Propagation as a Way of Life: A Framework for Bayesian Inference on Partitioned Data,” *Journal of Machine Learning Research*, 21, 1–53.
- Vovk, V., Gammerman, A., and Shafer, G. (2005), *Algorithmic learning in a random world*, Springer Science & Business Media.
- Wang, H., Li, G., and Jiang, G. (2007), “Robust Regression Shrinkage and Consistent Variable Selection Through the LAD-Lasso,” *Journal of Business and Economic Statistics*, 25, 347–355.
- Wang, X. and Leng, C. (2016), “High dimensional ordinary least squares projection for screening variables,” *Journal of the Royal Statistical Society. Series B (Statistical Methodology)*, 78, 589–611.
- Yang, E., Lozano, A. C., and Aravkin, A. (2018), “A general family of trimmed estimators for robust high-dimensional data analysis,” *Electronic Journal of Statistics*, 12, 3519–3553.
- Yourganov, G., Smith, K., Fridriksson, J., and Rorden, C. (2015), “Predicting aphasia type from brain damage measured with structural MRI,” *Cortex*, 73, 203–2015.
- Zhou, K., Li, K.-C., and Zhou, Q. (2021), “Honest confidence sets for high-dimensional

regression by projection and shrinkage,” *Journal of the American Statistical Association*, 1–20.

Zhou, L. and Zou, H. (2021), “Cross-Fitted Residual Regression for High-Dimensional Heteroscedasticity Pursuit,” *Journal of the American Statistical Association*, 0, 1–10.

Ziel, F. (2016), “Iteratively reweighted adaptive lasso for conditional heteroscedastic time series with applications to AR-ARCH type processes,” *Computational Statistics and Data Analysis*, 100, 773–793.

SUPPLEMENTARY MATERIAL

A Additional Simulation Results

We examined the performance of H-PROBE by focusing on the Root Mean Squared Error (RMSE, main text) and Median Absolute Deviation (MAD) of $\mathbf{X}'(\gamma\beta)$, where data \mathbf{X} consists of new observations not used during estimation (test set). Figure A.1 shows that for all simulation settings except one, H-PROBE had the lowest MAD, especially when the proportion of signals, the number of predictors on the mean, or the effect size of β were higher. Results are only shown for $\eta_\beta = 0.8$ for brevity. In the setting where H-PROBE slightly underperformed compared to PROBE, the MAD was 6% higher for H-PROBE.

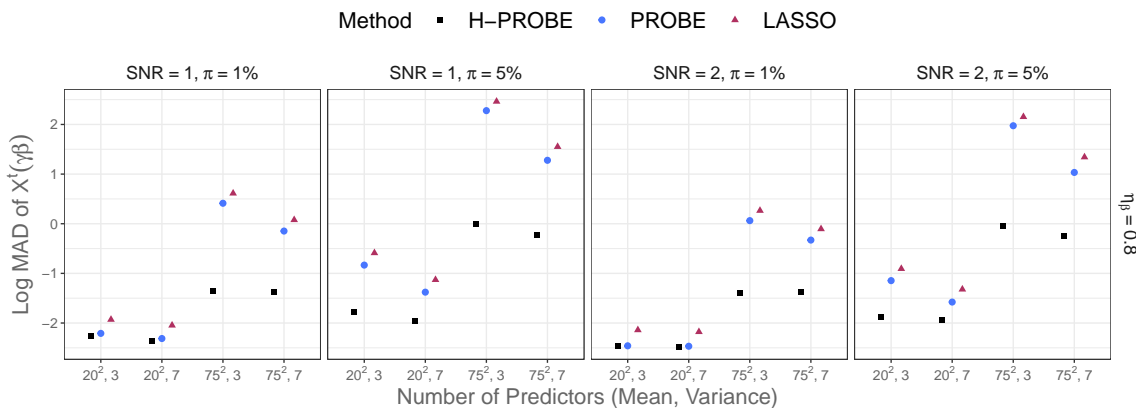


Figure A.1: Log Median Absolute Deviation (MAD) of $\mathbf{X}'(\gamma\beta)$ for H-PROBE (black squares), PROBE (blue circles), or LASSO (maroon triangles), for selected simulation settings.

Figure A.2 shows Prediction Interval (PI) lengths associated with the PI Empirical Coverage Probabilities (ECPs) in Figure 3. The PI lengths in the settings where PI ECPs for the PROBE method exceeded 95% were the widest, however, those ECPs did not actually cover the 0.95 level.

We also examined the bias and standard deviation of the $\tilde{\omega}$ coefficient estimates, from

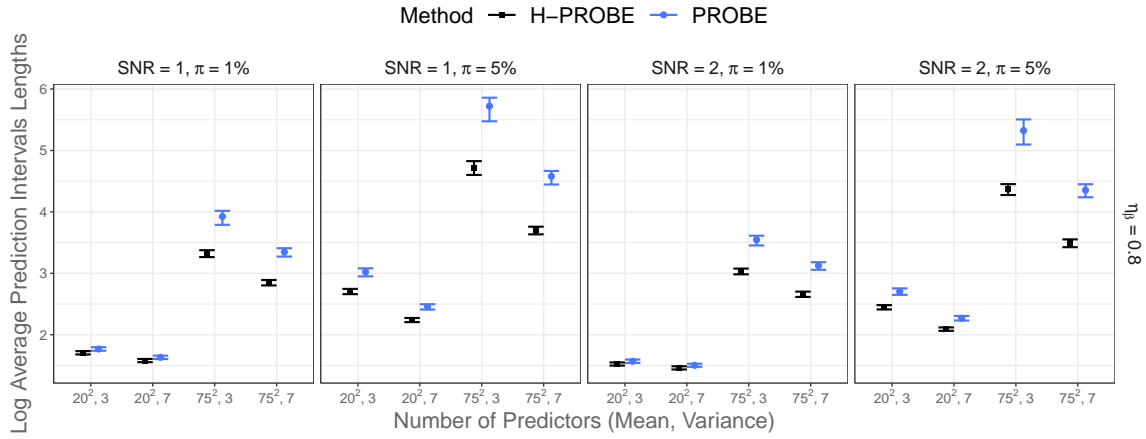


Figure A.2: Log Average Prediction Intervals (PI) lengths for $Y_{i,test}$ for H-PROBE (black squares) and PROBE (blue circles), for selected simulation settings. Vertical lines represent the first and third quartiles of the distributions of PI lengths.

the model on the variance. Figure A.3 shows the average bias for the intercept ω_1 , the first continuous coefficient ω_2 , and the first binary coefficient ω_3 , with the vertical bars indicating the minimum and maximum bias across v and SNR settings. The results are displayed by p , π , and η_β settings. In all settings, the bias was lower for first continuous and binary coefficients ω_2 and ω_3 , respectively, compared to intercept ω_1 . Generally, bias was more pronounced overall in the ultra high-dimensional setting ($p = 75^2$) with more true signals among the available predictors ($\pi = 5\%$). The standard deviation for intercept ω_1 and first binary coefficient ω_3 was higher than for continuous coefficient ω_2 in all settings.

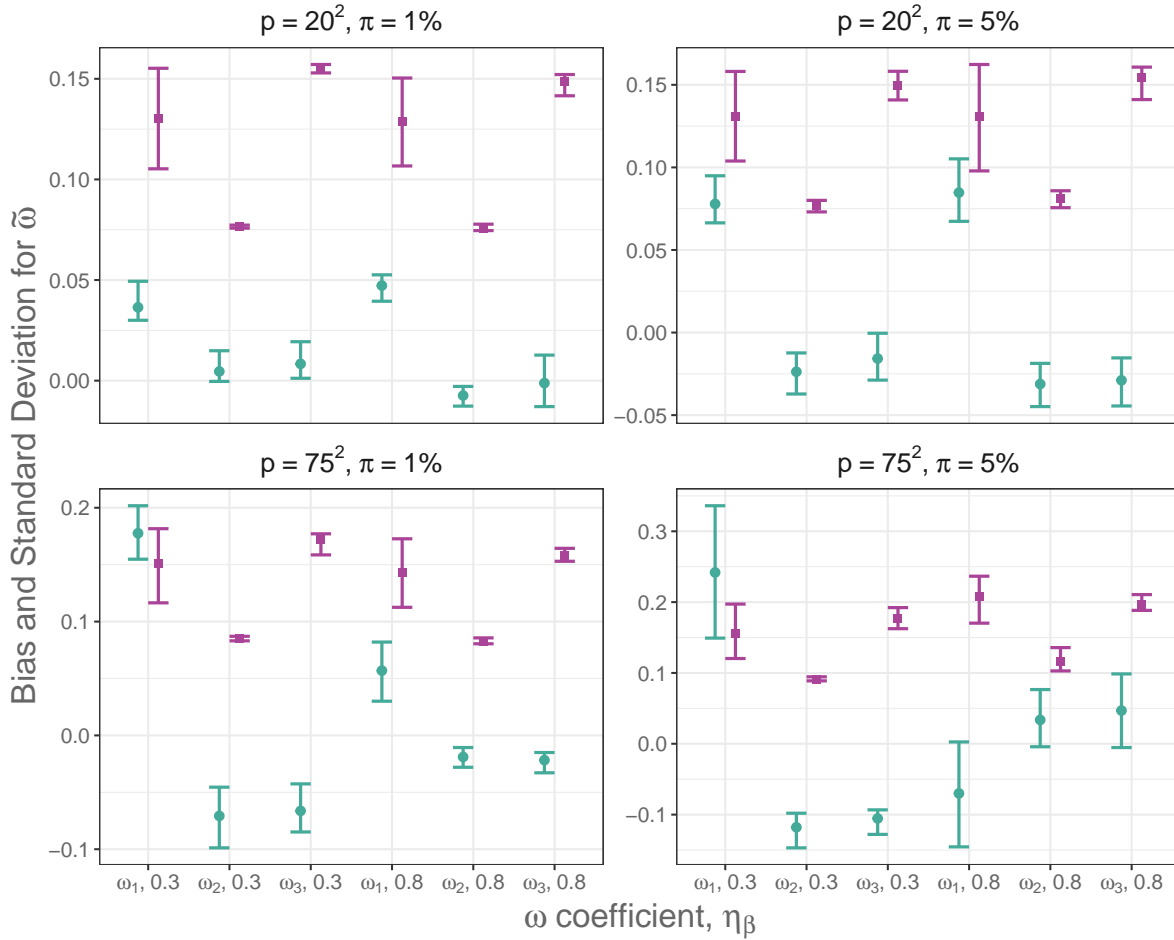


Figure A.3: Bias (green circle) and Standard Deviation (purple squares) of $\tilde{\omega}$ for H-PROBE. Vertical lines represent the minimum and maximum bias and standard deviations averaged across settings.

B Additional Data Analysis Results

Figure B.4 provides per-voxel statistical brain maps that compare the performance of H-PROBE to PROBE. There is a large overlap between the voxels with positive β estimates between the two approaches. These voxels appear to be located in and around the Inferior Frontal Gyrus, which contains Broca’s region, an important area of the brain linked to speech production. The LASSO model only resulted in negative β estimates. Since stroke injury is constrained by vasculature, and the presence of a brain injury is an inclusion criteria of the study data, negative β estimates for a given voxel indicate that the core

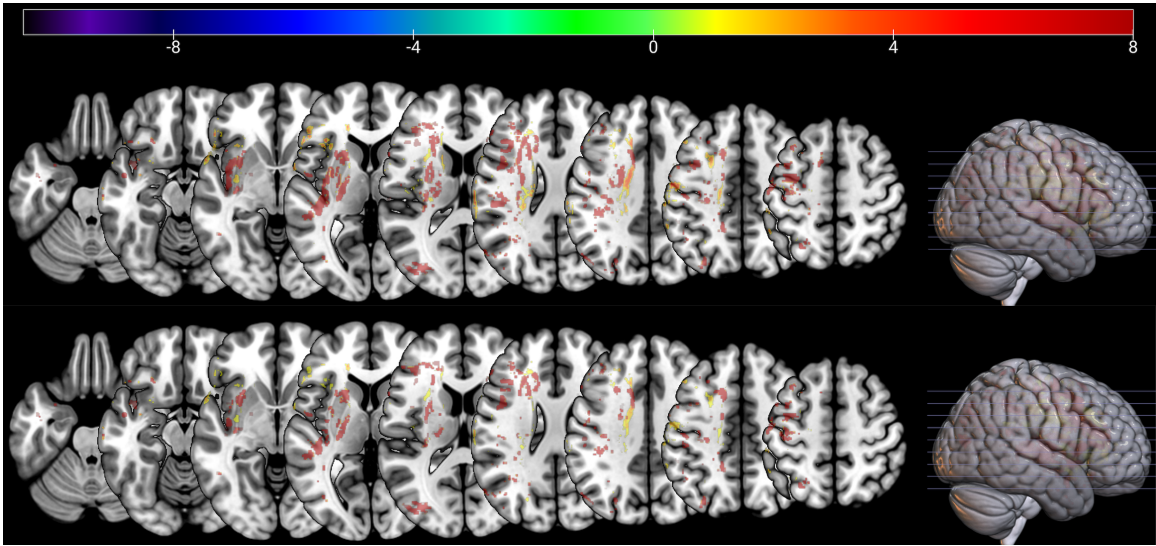


Figure B.4: Brain maps showing position, direction, and magnitude of voxel-specific β coefficients across different slides for PROBE (top) and H-PROBE (bottom). The color legend represents the value of β estimates (direction and magnitude).

brain modules related to speech have been spared.

To ensure that the non-linear relationship between the error variance σ_i^2 and total brain damage could not be remedied by a transformation of the Aphasia Quotient (AQ) outcome, we performed additional analysis examining transformations of AQ. We examined multiple transformations and provide figures for two of the transformations. We applied log and square root inverse transformations to AQ, $AQ_{log-inv} = \log\left(\frac{100-AQ}{100}\right)$ and $AQ_{sqr-inv} = \sqrt{\left(\frac{100-AQ}{100}\right)}$, and modeled $AQ_{log-inv}$, $AQ_{sqr-inv}$ using the PROBE method, a homoscedastic approach. Figure B.5 shows that despite of both transformations shown, the non-linearity of the relationship between the error variance σ_i^2 and total brain damage remains. This result remained in other transformations we examined.

Figure B.6 shows that H-PROBE provides predictions \hat{Y}_i that have a different range for distinct values of estimated $\tilde{\sigma}_i^2$. This important characteristic of heteroscedastic data is not detected by PROBE.

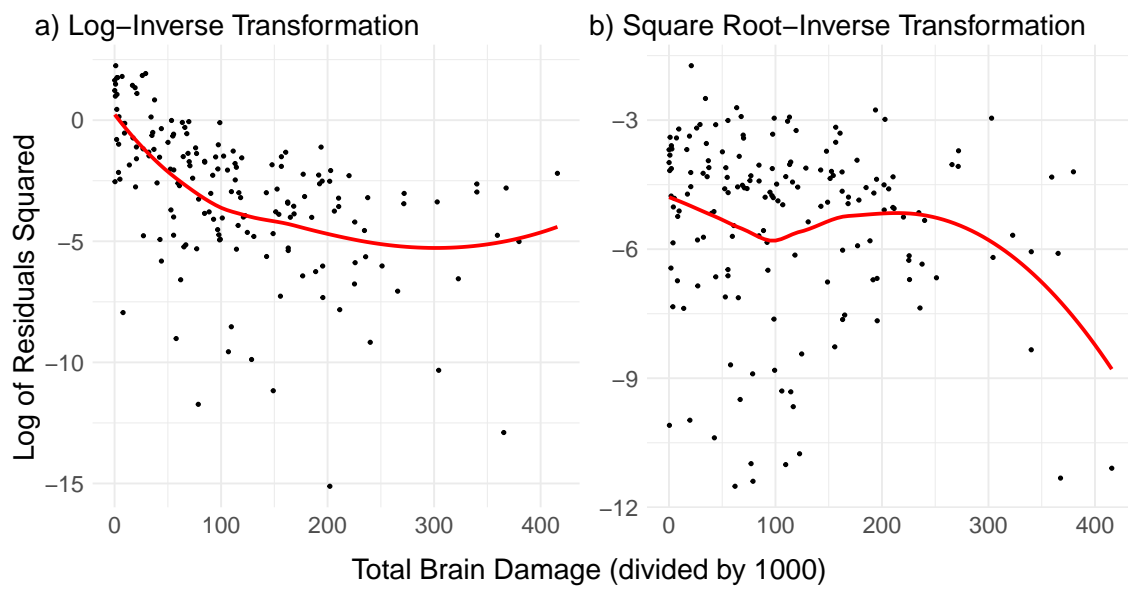


Figure B.5: (a) Log Residuals Squared from PROBE using brain images as predictors and the transformed outcome $AQ_{log-inv}$. (b) Log Residuals Squared from PROBE using brain images as predictors and the transformed outcome $AQ_{sqrt-inv}$

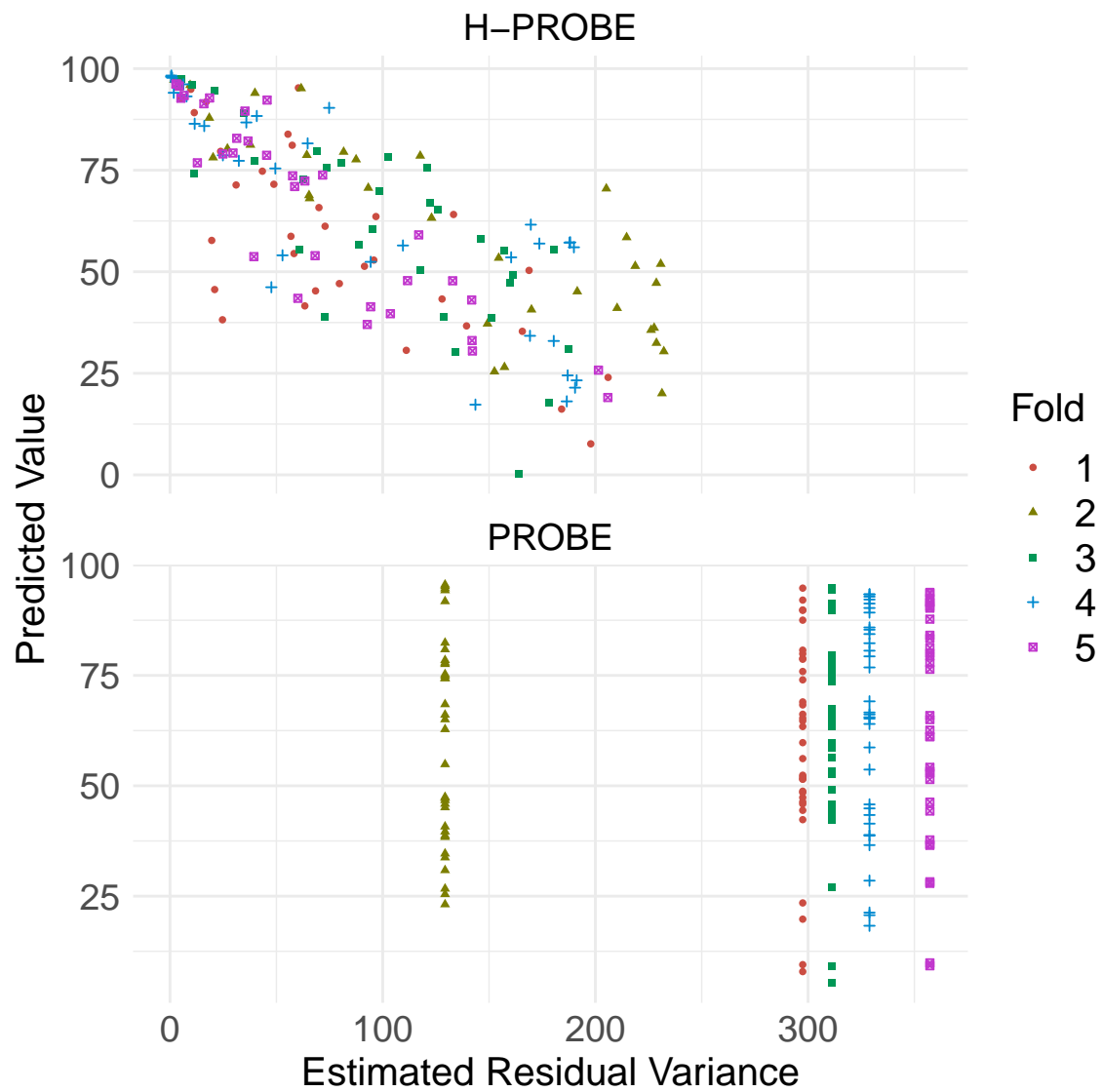


Figure B.6: Predicted Values \hat{Y}_i by estimated $\hat{\sigma}_i^2$ using H-PROBE and PROBE. Note that within a given fold, $\hat{\sigma}_i^2$ estimates for observation i are the same when using PROBE. The color legend represents the cross-validation fold in which predictions were obtained.